# COMPARISON OF TWO POST-PROCESSING TECHNIQUES IN 2D FEM BASED ON LOCAL SOLUTIONS OF THE LAPLACE EQUATION

U. Pahner, R. Mertens, K. Hameyer, R. Belmans
KU Leuven, Dept. EE (ESAT), Div. ELEN,
K.-Mercierlaan 94, 3001 Heverlee,
Belgium

**Abstract**
Reliable 2D force calculation algorithms are essential in the analysis of electromagnetic devices and actuators. Algorithms like virtual work, the Maxwell stress tensor and the Lorenz force method are in common use with the finite element method (FEM). A local post-process has been introduced [1, 2, 3, 7] promising a higher accuracy when compared to the conventional techniques. This paper compares two derived methods for local post-processing and their application to force and torque calculations of electrical machines and actuators. The algorithms are based on the solution of the Laplace equation in air regions, using the vector potential distribution from a finite element solution as their boundary condition. Advantages as well as limitations are discussed.

## Introduction

Most of the classical force calculation methods have their disadvantages regarding computational expense (minimum two FEM calculations for virtual work) or numerical accuracy (Maxwell stress tensor). Using adaptive mesh refinement, the accuracy of the Maxwell stress computation on a given contour can be enhanced, but the computational cost is increasing dramatically. The method proposed in [2, 3] offers a good compromise for practical applications. Low order elements, combined with a limited number of adaptive mesh refinement steps lead to a more accurate force computation when compared to the conventional Maxwell stress method. Two derived methods are presented here.

## Local post-processing based on the Laplace equation

Using the 2D finite element method, a vector potential solution $A_z(x,y)$ is obtained. Assuming first order triangular elements, the variation of $A_z$ inside one finite element is:

$$A_z(x,y) = \alpha_1 + \alpha_2 x + \alpha_3 y \tag{1}$$

The coefficients $\alpha_1$, $\alpha_2$ and $\alpha_3$ are computed using the nodal co-ordinates and the nodal vector potentials.
To compute the forces according to the Maxwell stress tensor, the local values of flux density have to be evaluated. The formulas for the normal and tangential component of the force along a contour *C* can be derived from the Maxwell stress tensor.

$$F_n = \frac{1}{2\mu_0}\int_C \left(B_n^2 - B_t^2\right) \mathrm{d}s \tag{2}$$

$$F_t = \frac{1}{\mu_0}\int_C B_n B_t \,\mathrm{d}s \tag{3}$$

The flux density components inside one element are derived from the nodal vector potentials. The x-component of *B*, as an example, is calculated as follows:

$$B_x = \frac{\partial A_z}{\partial y} = \frac{1}{2\Delta}\sum_i^k c_i A_{zi} = \text{const} \tag{4}$$

Thus, the order of *B* is of one less than the order of the vector potential. The numerical inaccuracy of the classical Maxwell stress method arises from this loss of accuracy due to numerical differentiation. Using standard linear shape functions to approximate the continuous vector potential over a triangular finite element results in a piece wise constant magnetic flux density.

Consider the solution of the Laplace equation $\nabla^2 A = 0$ in a source free region, given as a series of circular harmonics of order *k* [1]:

$$A_z(r,\vartheta) = \frac{a_0}{2} + \sum_{k=1}^{M}\Big(a_k r^k \cos(k\vartheta) + b_k r^k \sin(k\vartheta) + c_k r^{-k}\cos(k\vartheta) + d_k r^{-k}\sin(k\vartheta)\Big) \tag{5}$$

Two methods can be derived using this formula as a basis: Method I, describing the local solution inside a series of circles along a contour and method II, describing the solution inside two concentric circles.

## Method I

The first method [2, 3, 7] uses the known values of the magnetic vector potential on a circle with radius *R* as boundary conditions. The local field value at the centre point *p* of the circular source free region is calculated. This centre point is part of a contour *C* of arbitrary shape (Fig. 1).
The distance of the centre points on the contour are chosen such that the circles overlap. Because of the

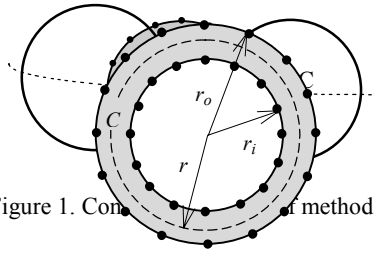


Figure 1. Con… of method I.

Figure 2. Considered domain of method II.

finite value of the magnetic vector potential in the centre point $p$ ($r = 0$), the coefficients $c_k$ and $d_k$ are zero. The coefficients $a_k$ and $b_k$ from eq. (5) can be determined by using the known potentials $A(R,\vartheta)$ on the circumference of a circle with radius $R$ .

$$a_k = \frac{1}{\pi R^k}\int_0^{2\pi} A(R,\vartheta)\cdot\cos(k\vartheta)\,\mathrm{d}\vartheta$$
$$b_k = \frac{1}{\pi R^k}\int_0^{2\pi} A(R,\vartheta)\cdot\sin(k\vartheta)\,\mathrm{d}\vartheta \qquad (6)$$

Now a finite number of $N$ equi-angularly ordered points is applied onto the circumference of the circle.

$$A_i(R,\vartheta_i) = A(R, i\cdot\tfrac{2\pi}{N}) \quad , \; i = 1(1)N \qquad (7)$$

The Fourier coefficients are rewritten as follows:

$$a_k = \frac{2}{N\cdot R^k}\sum_{i=1}^{N} A_i\cos(k\vartheta_i)$$
$$b_k = \frac{2}{N\cdot R^k}\sum_{i=1}^{N} A_i\sin(k\vartheta_i) \qquad (8)$$

With the series eq. (5) and their coefficients eqs. (8), the potential in the centre of a circle can be computed by only knowing the boundary potential values on the circumference of the circle. Using this approach inside a source free region of a finite element solution, the value of the potential of the field point $p$ is now depending on the solution in several finite elements. Thus, local numerical errors in single elements will have a relatively small influence on the solution in the considered field point. As the value for the magnetic flux density (instead of the potential) at the centre point is necessary to calculate the force, the derivatives of eq. (5) are computed. The $a_0$-term of eq. (5) vanishes. Due to the arbitrary shape of the contour, the magnetic flux density is decomposed in its $x$- and $y$-components.

$$B_x = \left.\frac{\partial A_z(x,y)}{\partial y}\right|_p = b_1 \qquad (9a)$$

$$B_y = -\left.\frac{\partial A_z(x,y)}{\partial x}\right|_p = -a_1 \qquad (9b)$$

The components of B can directly be calculated using eqs. (8) and (9a, 9b). The implementation of this algorithm into a post-processing code is straight forward. The computation time is dominated by the element search algorithm.

**Method II**

The second method [7] uses the values of the magnetic vector potential on two concentric circles with radii $r_i$ and $r_o$ as boundary conditions (Fig. 2). Local field values on the circular contour $C$ with radius $r_i < r < r_o$ are calculated.

If the inner radius $r_i$ is taken as reference and $a_0$ from eq. (5) is assumed to be zero, the general solution of Laplace's equation is

$$A_z(r,\vartheta) = \sum_{k=1}^{M}\left( a_k\left(\frac{r}{r_i}\right)^k\cos(k\vartheta) + b_k\left(\frac{r}{r_i}\right)^k\sin(k\vartheta) + c_k\left(\frac{r_i}{r}\right)^k\cos(k\vartheta) + d_k\left(\frac{r_i}{r}\right)^k\sin(k\vartheta)\right) \qquad (10)$$

The coefficients $a_k$, $b_k$, $c_k$ and $d_k$ are independently determined for each circular harmonic. An FFT algorithm is used to express the magnetic vector potential at the boundaries as a series of such circular harmonics.

$$A_z(r_i,\vartheta) = \sum_{k=1}^{M}\left(a_{k,i}\cos(k\vartheta) + b_{k,i}\sin(k\vartheta)\right) \qquad (11a)$$

$$A_z(r_o,\vartheta) = \sum_{k=1}^{M}\left(a_{k,o}\cos(k\vartheta) + b_{k,o}\sin(k\vartheta)\right) \qquad (11b)$$

$$\begin{bmatrix} 1 & 1 \\ \left(\frac{r_o}{r_i}\right)^k & \left(\frac{r_i}{r_o}\right)^k \end{bmatrix}\begin{bmatrix} a_k \\ c_k \end{bmatrix} = \begin{bmatrix} a_{k,i} \\ a_{k,o} \end{bmatrix} \qquad (12a)$$

$$\begin{bmatrix} 1 & 1 \\ \left(\frac{r_o}{r_i}\right)^k & \left(\frac{r_i}{r_o}\right)^k \end{bmatrix}\begin{bmatrix} b_k \\ d_k \end{bmatrix} = \begin{bmatrix} b_{k,i} \\ b_{k,o} \end{bmatrix} \qquad (12b)$$

Therefore, as the magnetic vector potential is known at points along two contours with radius $r_i$ and $r_o$, the coefficients $a_{ki}$, $a_{ko}$, $b_{ki}$ and $b_{ko}$ in eqs. (11a, 11b) are determined using the FFT algorithm. The coefficients $a_k$, $b_k$, $c_k$ and $d_k$ from eq. (10) follow from the eqs. (12a, 12b). Once the expression of the magnetic vector potential along contour $C$ is found, the normal and tangential component of the magnetic flux density can be determined.

$$B_n(r,\vartheta) = \sum_{k=1}^{M}\left( -k\,a_k\frac{r^{k-1}}{r_i^k}\sin(k\vartheta) + k\,b_k\frac{r^{k-1}}{r_i^k}\cos(k\vartheta) - k\,c_k\frac{r_i^k}{r^{k+1}}\sin(k\vartheta) + k\,d_k\frac{r_i^k}{r^{k+1}}\cos(k\vartheta)\right) \qquad (13a)$$

$$B_t(r,\vartheta) = \sum_{k=1}^{M}\left( -k\,a_k\frac{r^{k-1}}{r_i^k}\cos(k\vartheta) - k\,b_k\frac{r^{k-1}}{r_i^k}\sin(k\vartheta) + k\,c_k\frac{r_i^k}{r^{k+1}}\cos(k\vartheta) + k\,d_k\frac{r_i^k}{r^{k+1}}\sin(k\vartheta)\right) \qquad (13b)$$

)

The tangential force component $F_t$ results in the torque $T$ of the device. It can be shown that the value of the torque is given by eq. (14) and is independent of the radius $r$ of contour $C$. It is not necessary to calculate the normal and tangential component of the magnetic flux density on the contour. This results in a faster algorithm.

$$T = \frac{2\pi}{\mu_0} \sum_{k=1}^{M} \left( k^2 \left( b_k \, c_k - a_k \, d_k \right) \right) \qquad (14)$$

## Applicability

Advantages and limits of both methods decide on their applicability to various types of actuators. Method I is preferred for the force computation on arbitrary shaped contours, as method II does not allow a free shape of a contour. Method II has its clear advantage in the analysis of rotationally symmetrical devices, in particular rotating machines. Method I suffers here from increased computational expense, because a large number of small overlapping local circles along the contour inside the air gap. Realistic motors have a very small air gap is necessary. The radius of the local post-processing regions must be chosen small enough to be placed entirely inside the air gap which would increase the number of circles dramatically. Therefore method II is then chosen instead.

## Numerical results

### Method I

The attracting force acting on a body is computed using method I. Method I is compared to the results of conventional post-processing. Consider a simple iron C-core actuator [5] with an iron armature some short distance away, as shown in figure 3.

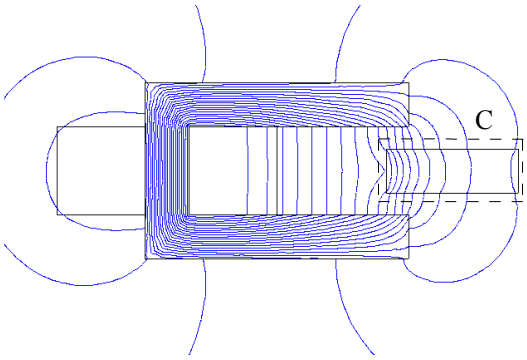


Figure 3. C-core actuator with iron armature.

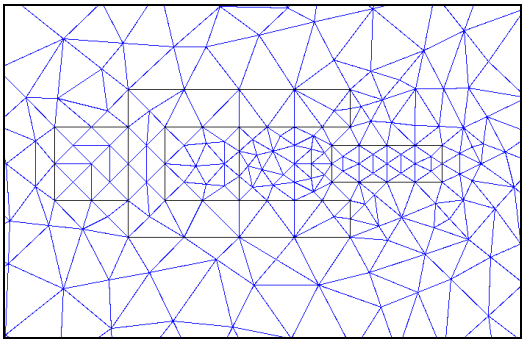

a) initial mesh (274 nodes, 524 elements, elapsed solution time 0.6 s)

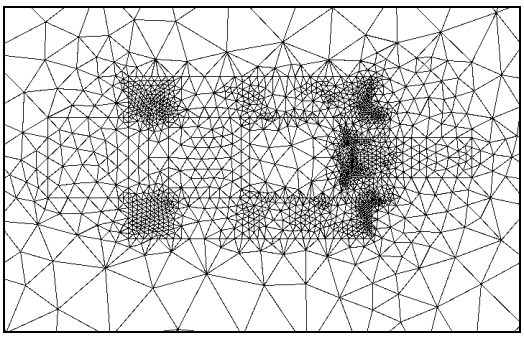

b) adaption step 3 (1698 nodes, 3372 elements, elapsed solution time 21s)

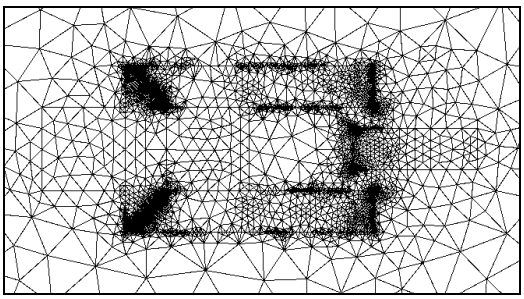

c) adaption step 6 (7486 nodes, 14948 elements, elapsed solution time 3:53 min)

Figure 4. Discretisation after a selected number of mesh refinement steps.

As the C-core iron is highly saturated, a non-linear magnetostatic analysis is required. The force on the actuator is computed along the closed path C. To compare the performance of the enhanced force calculation method I to the classical Maxwell stress method, a number of calculations using a mesh adaption scheme are carried out. Figure 4 illustrates the discretisation found at a selected number of refinement steps.

1800 equidistant points along the integration path are chosen for the classical Maxwell stress method. The distance of the center points of the circles for method I is equal to the radius of the circles. 15 equiangular sample points are taken on each circle, resulting in 1500 points in total. The elapsed computation time for both methods will be similar in this case, as the element search routine is the dominating part of the algorithms with regard to the computational expense.

The calculations are carried out on an HP 715-50 and the elapsed computation time includes the I/O of the solution data (table 1-1, 1-2).

Table 1-1: Solution data for different refinement steps.

| nb. of steps | nb. of nodes | nb. of elements | stored magnetic energy [J] | magn. co-energy [J] |
|---|---|---|---|---|
| 0 | 274 | 524 | 40.30 | 51.06 |
| 1 | 577 | 1130 | 40.80 | 52.90 |
| 2 | 914 | 1804 | 41.08 | 53.14 |
| 3 | 1698 | 3372 | 41.10 | 53.45 |
| 4 | 2613 | 5202 | 41.15 | 53.60 |
| 5 | 3835 | 7646 | 41.17 | 53.62 |
| 6 | 7486 | 14948 | 41.18 | 53.66 |

Table 1-2: Elapsed times for solution and post-process.

| nb. of steps | FEM-solution [s] | post-process [s] |
|---|---|---|
| 0 | 1 | 1 |
| 1 | 5 | 2 |
| 2 | 9 | 2.5 |
| 3 | 21 | 3 |
| 4 | 44 | 3.5 |
| 5 | 90 | 5 |
| 6 | 233 | 7 |

From the physics of the model (Fig. 3), an x-component of the force is expected, whereas the y-component should be zero. Figure 5 and 6 illustrate the performance of the methods.

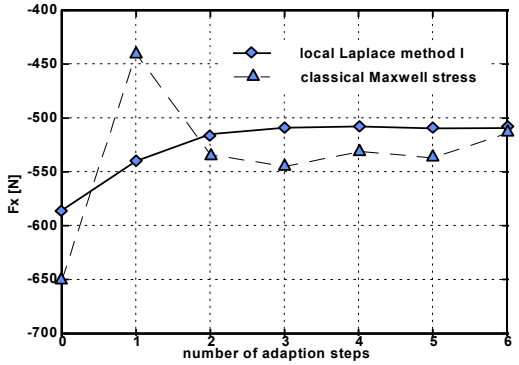


Figure 5. X-component of the attracting force evaluated along contour C in figure 3.

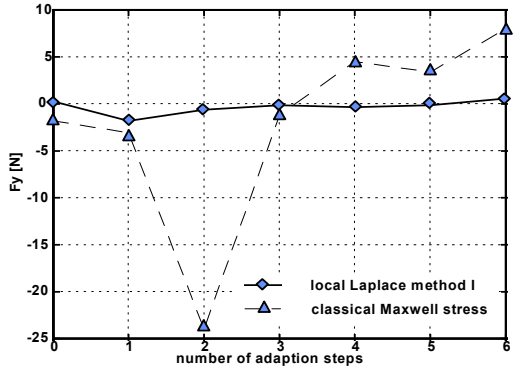


Figure 6. Y-component of the force (theoretically zero).

The only tunable parameters of the algorithm of method I (eq. 8) are the number of points *N* on the circumference of the local circles, the radius *R* and the distance between centre points of neighbouring centres. It has been found that more than 20 points on the circumference of the circle do not lead to any improvement of the convergence of the method. The distance between the centre points of two neighbouring circles is chosen as the radius, leading to an intersection of three circles. The most crucial parameter is the radius of the circle. It should always be chosen as large as possible, which allows the method to sample the finite element solution in as many different elements as possible. As a worst case, the circles could be much smaller than the elements in the region, leading to the solution of the classical Maxwell stress method.

In [2,3], the rate of convergence for this method has been investigated. Figure 7 shows the convergence of the relative error of the x-component for this C-core model.

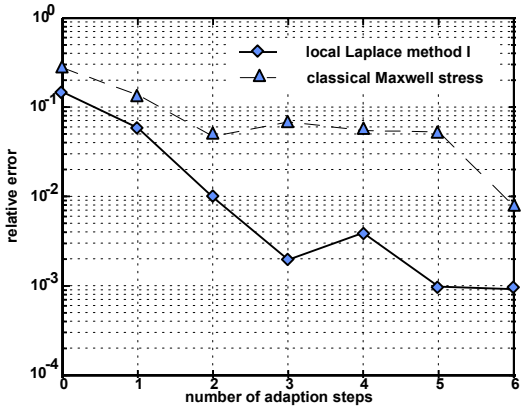


Figure 7. Rate of convergence of the relative error for both methods compared.

**Method II**

The torque of an 400 kW induction machine is calculated using method II (Fig. 8, Table 2). A comparison with measured data and the classical Maxwell stress method is carried out.

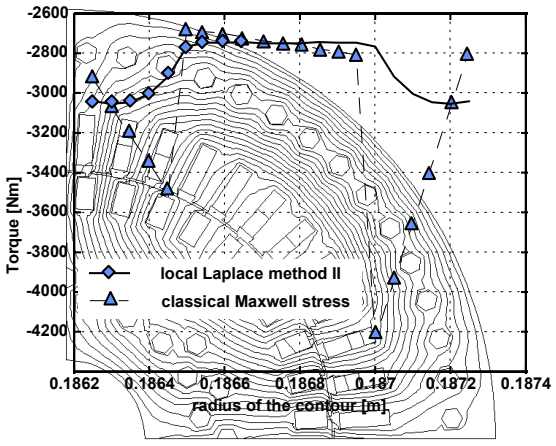


Figure 10. Variation of the torque calculated along different contours inside the air gap of the solution (400 kW induction motor).

Figure 8. Equi-potential plot of the real component

For the FEM-analysis, a non-linear time-harmonic analysis is performed [6].

Table 2. Data of the 400 kW induction machine [6].

| machine data |
|---|

| | |
|---|---|
| voltage | 0-1950 V |
| rated current | 154 A |
| rated power | 402 kW |
| cos φ | 0.91 |
| rpm | 0-4350 |
| frequency | 0-140 Hz |
| number of pole pairs | 2 |
| number of stator slots | 48 |
| number of rotor slots | 40 |
| outer diameter | 60 cm |
| air gap length | 1.5 mm |
| | |
| Measured torque | $T_m$ = 2733 Nm |

As indicated for method I, a good trade-off between mesh refinement and the enhanced post-processing methods is necessary to ensure accurate results. A different approach is taken here. A relatively coarse discretisation in the air gap is chosen (Fig. 9), using no adaptive refinement, but providing at least three uniform layers of elements between rotor and stator.

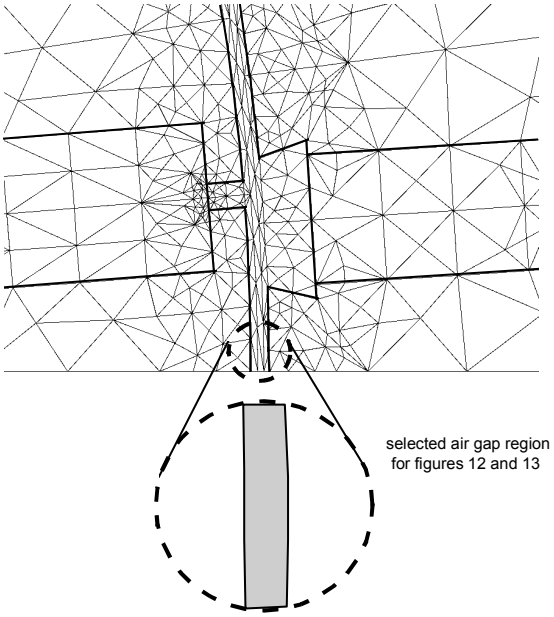


Figure 9. Discretisation inside the air gap.

Even with such a coarse discretisation, the Laplace based method II is less sensitive to the actual choice of the contour inside the air gap then the classical method. The air gap spans a region between an inner radius of 0.186 m up to an outer radius of 0.1875 m. Figure 10 shows the variation of the calculated torque. Contours with different radii are chosen. For the Laplace based method II, the inner and outer radii are varied simultaneously. Therefore, the value of the torque varies symmetrically towards the middle of the air gap.

The variation of the calculated torque's using method II is much smaller when compared to the classical method. It must be stated, however, that an appropriate mesh refinement scheme would lead to even better results.

The main indication of the strength of the Laplace based method is shown in figure 11. The number of sample points for both methods is varied and the results are compared in terms of the rate of convergence of the relative error.

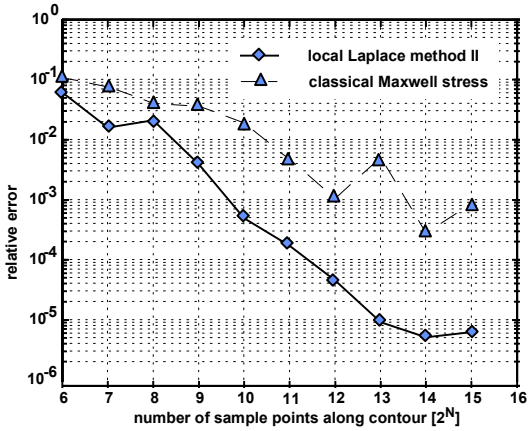


Figure 11. Rate of convergence of the relative error. (Variation of the number of sample points)

The rate of convergence of the relative error indicates that the necessary number of sample points for method II can be chosen substantially less then for the classical method. As shown in figure 11, the best relative error is computed with 16384 points using Maxwell, instead of 2048 points using method II. Typical computation times for this model are

| | | |
|---|---|---|
| Model | : 4659 nodes, 9178 elements | |
| Maxwell | : 16384 points | - 1:12 min |
| Method II | : 2048 points | - 24 s |

Again, the element search algorithm is the dominating part with regard to the computation time.

Even so the local components of the flux density (eqs. 13a, 13b) need not to be evaluated explicitly for method II, the variation of B is shown in figure 12. Comparing figure 12 with figure 13, it is obvious that the new post-processing method promises higher accuracy for an algorithm based on derived local field values.

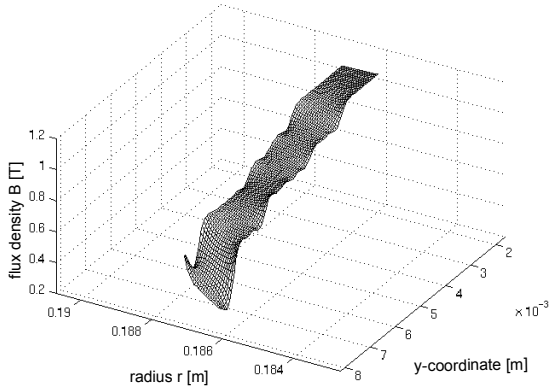


Figure 12. Variation of B inside the selected air gap region (Fig. 9) using derivatives of the general solution of Laplace's equation (eq. 10).

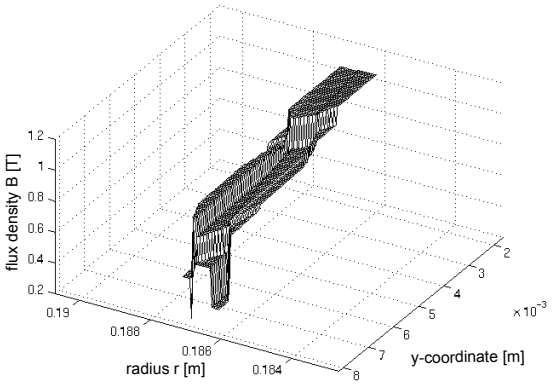


Figure 13. Variation of B inside the selected air gap region (Fig. 9), using numerical derivatives.

## Conclusion

Two force calculation methods, based on local solutions of the Laplace equation are presented and compared with the classical Maxwell stress method. Both methods allow a higher accuracy of the force calculation. They are easy to implement and the total computational expense is acceptable. Using one of the two methods together with low order finite elements and h-type adaption are resulting in fast and accurate computations. The reduction of numerical errors at low computational cost is of utmost importance for automatic optimization routines. Due to the higher rate of convergence of both methods, optimizations involving force computations need less iterations. An implementation of similar algorithms in three dimensions and for the solution of Poisson's equation is under investigation.


## Acknowledgment

The authors are grateful to the Belgian Nationaal Fonds voor Wetenschappelijk Onderzoek for its financial support of this work and the Belgian Ministry of Scientific Research for granting the IUAP No. 51 on Magnetic Fields.


## References


[1] K.J. Binns, P.J. Lawrenson, C.W. Trowbridge, 'The Analytical and Numerical Solution of Electric and Magnetic Fields', John Wiley & Sons, 1992.

[2] J. Franz, M. Kasper, 'Superconvergent finite element solutions of Laplace and Poisson equation', COMPUMAG, Berlin, pp. 64-65, July 1995.

[3] M. Kasper, J. Franz, 'Highly accurate computation of field quantities and forces by superconvergence in finite elements', IEEE Transactions on Magnetics, May 1994.

[4] P.P.Silvester and D. Omeragic, 'Differentiation of finite element solutions of Poisson equation', IEEE Transactions on Magnetics, vol. 29, pp. 1993-1996, March 1993.

[5] E. M. Freeman, R.A. Ashen, 'Force calculation in magnetic field problems using virtual work with only one solution', Proceedings of the Sixt IEE International conference on Electrical Machines and Drives, Oxford, UK, 1993, pp. 318-322.

[6] R. De Weerdt, K. Brandiski, U. Pahner and R. Belmans, 'Comparative analysis of two methods for the time-harmonic solution of the stady state in induction motors', J. of Applied Physics. 75 (10), Proc. of the 38th Annual Conference on Magnetism and Magnetic Materials, p. 6050 f.

[7] R. Mertens, R. De Weerdt, U. Pahner, K. Hameyer and R. Belmans,'Force calculation based on a local solution of Laplace's equation', Proc. of the IEEE Conf. on Electromagnetic Field Computation, Okayama, Japan, March 18-20, 1996, p.354.